

Femtoscopic study of the kaon-deuteron interaction

Author: Esteve Cabré Coll-Vinent

Facultat de Física, Universitat de Barcelona, Diagonal 645, 08028 Barcelona, Spain.

Advisors: Juan Torres Rincón and Àngels Ramos

Abstract: The kaon-deuteron interaction has been studied through different models. The one developed in this work constructs the K^-d interaction by folding K^-n and K^-p local potentials derived from a chiral effective Lagrangian. This approach is probed using the femtoscopy technique and the K^-d correlation function data provided by the ALICE collaboration @ LHC. Results show an excellent agreement with experimental data and provide evidence of a quasi-bound state inherited from the $\Lambda(1405)$ resonance, and also lay out further possibilities of improving the model to constrain the physical values of the femtoscopic source.

Keywords: Scattering theory; femtoscopy; Schrödinger equation

SDGs: Quality education; Industry, innovation and infrastructure; Partnerships for the goals

I. INTRODUCTION

Accessing the residual strong interaction among hadrons through femtoscopy has been the focus of a lot of research in recent years [1]. Correlation functions in momentum space have been particularly useful ([1], [2], [3]) in relativistic heavy-ion collisions (RHIC) facilities to study the interactions of unstable particles, such as kaons or hyperons, whose beam realization is difficult and thus lack scattering data. This work focuses on probing a folding method to model the kaon-deuteron interaction, employing a $\bar{K}N$ potential constructed from chiral effective field theory (χ EFT) in a local description. The K^-d potential (V_{K^-d}) is then used to solve the Schrödinger equation (SE) with the inclusion of electromagnetic effects. The resulting wave function is analysed and employed to obtain the correlation function, which will be compared with available experimental data from ALICE, an international collaboration at CERN's LHC.

Section II in this work will cover the theoretical formalism involved in computing the $\bar{K}N$ strong potential, which is reduced to equivalent single-channel local potentials in charge basis, V_{K^-n} and V_{K^-p} , so these can be folded to obtain V_{K^-d} . It also covers some scattering theory and femtoscopy concepts necessary to interpret the results, which are introduced in Sec. III for V_{K^-d} and the wave and correlation functions. Finally, in Sec. IV the conclusions are formulated on this informed two-body model for the K^-d interaction. In Appendix A, the reduction to single-channel potentials is discussed in more detail, as is the potential folding in Appendix B. Natural units, with $\hbar = c = 1$, are used throughout this work.

II. FORMALISM

A. Coupled-channel T matrix equation and V_{11}^{eff}

The starting point is the meson-baryon χ EFT [4], whose lowest-order Lagrangian allows to derive a $\bar{K}N$

strong interaction that contains elastic and inelastic cross-sections with coupled channels; for isospin $I = 0$ there are 4 of them ($\bar{K}N, \pi\Sigma, \eta\Lambda, K\Xi$) and for $I = 1$ there are 5 ($\bar{K}N, \pi\Sigma, \pi\Lambda, \eta\Sigma$ and $K\Xi$). The lowest-order amplitude for an invariant mass \sqrt{s} , $V_{ij}(\sqrt{s})$, where i and j indicate the incoming and outgoing channels, respectively, is evaluated from the Lagrangian and then used in the coupled-channel T -matrix equation,

$$T_{ij}(\sqrt{s}) = V_{ij}(\sqrt{s}) + V_{il}(\sqrt{s})G_l(\sqrt{s})T_{lj}(\sqrt{s}), \quad (1)$$

where $T_{ij}(\sqrt{s})$ is the s -wave projected scattering amplitude or T -matrix element for the initial and final channels ij .

To avoid working in a coupled-channel basis, a single-channel equivalent potential can be constructed, following Ref. [5], by applying the following expression (see details in Appendix A):

$$V_{11}^{\text{eff}} = V_{11} + \sum_{m=2}^N V_{1m}G_m V_{m1} + \sum_{m,l=2}^N V_{1m}G_m \tilde{T}_{ml} G_l V_{l1}, \quad (2)$$

with $N = 4, 5$ for the isospin channels $I = 0, 1$, respectively. The subindices 11 refer to the $\bar{K}N - \bar{K}N$ channel.

After transforming from the isospin to the physical basis, construction of an equivalent energy-dependent potential in coordinate space is carried out following the prescription in [6], leading to

$$V_{K^-i}(r; \sqrt{s}) = g(r)N(\sqrt{s})V_{K^-i}^{\text{eff}}(\sqrt{s}), \quad i = n, p, \quad (3)$$

where $N(\sqrt{s}) = M_N/(2\mu\sqrt{s})$ is an appropriate kinematic flux factor, with M_N being the nucleon mass and μ the reduced mass of the $\bar{K}N$ system, and $g(r)$ is a regulating Gaussian function,

$$g(r) = \frac{1}{\pi^{3/2}b^3} e^{-r^2/b^2}. \quad (4)$$

The parameter $b = 0.52$ fm is fixed by matching the $\bar{K}N$ scattering amplitude obtained by solving the single-channel SE using this local potential to the one obtained using the full Eq. (1). The results are found insensitive to a 20% variation of this parameter.

B. Potential folding

Motivated by Ref. [7], V_{K-d} is obtained by folding V_{K-p} and V_{K-n} over the distribution of p and n in the deuteron, respectively, which are assumed to be given by the deuteron density, $\rho_d(r)$, with the resulting potential spherically symmetric. The method is implemented through the following integral (see details in Appendix B), with $r_{\pm} \equiv |\mathbf{r} \pm \frac{1}{2}\mathbf{r}'|$:

$$V_{K-d}^S(r; \sqrt{s}) = \int d^3r' \rho_d(r') \left[V_{K-p}(r_-) + V_{K-n}(r_+) \right], \quad (5)$$

where r is the distance of the K^- to the centre of the deuteron and the superscript S stands for the strong (short-range) interaction. The electromagnetic interaction between two charged particles will also be taken into account, so a Coulomb potential term must be added,

$$V_{K-d}(r; \sqrt{s}) = V_{K-d}^S(r; \sqrt{s}) - \frac{\alpha}{r}, \quad (6)$$

where $\alpha = 1/137$ is the fine structure constant.

C. Scattering theory

To explore the validity of the total potential, the SE is now used with (6) to numerically calculate the K^-d wave function. As it is spherically symmetric, the SE reads,

$$\left(\frac{d}{dr^2} - k^2 + U(r; \sqrt{s}) - \frac{l(l+1)}{r^2} \right) u_l(r) = 0, \quad (7)$$

where $u_l(r)$ is the reduced radial wave function, k the relative momentum between the pair and $U(r; \sqrt{s}) = 2\mu_{K-d}V_{K-d}(r; \sqrt{s})$, with $\mu_{K-d} = \frac{m_{K^-}m_d}{m_{K^-}+m_d}$. As outlined in [8], in the low-energy limit in which k is small, the angular components with $l > 0$ should not affect the interaction as particles are unable to overcome the centrifugal barrier, so we will only take into account the $l = 0$ (or s -wave) component, $u_0(r)$. The Numerov algorithm, a finite difference method (see also [8]), is then used to solve Eq. (7) from $r = 0$, where $u_0(r) = 0$, outwards to R , an asymptotic value larger than the potential range.

The obtained wave function $u_0(r < R)$, which represents a scattering state, needs to be matched to the s -wave asymptotic partial wave, expressed using spherical Bessel (j_0) and Neumann (n_0) functions as

$$u_0^S(r; k) \stackrel{r \rightarrow \infty}{\equiv} r e^{i\delta_0} [\cos\delta_0 j_0(kr) - \sin\delta_0 n_0(kr)]. \quad (8)$$

The information about the interaction that happens inside the potential range is encoded in the asymptotic phase shift $\delta_0(k)$, which can be physically interpreted as a phase between $u_0(r \rightarrow \infty)$ and the free particle s -wave, $j_0(kr)$. The matching at $r = R$ of the wave functions and their derivatives is made through the comparison of their

logarithmic derivatives, $\beta_0 \equiv \left[r \frac{u_0'(r)}{u_0(r)} \right]_{r=R}$ resulting in the following expression for the phase shift,

$$\cot\delta_0 = \frac{kRn_0'(kR) - (\beta_0 - 1)n_0(kR)}{kRj_0'(kR) - (\beta_0 - 1)j_0(kR)}. \quad (9)$$

Note, however, that in the K^-d case electromagnetic effects need to be added, and it is the Coulomb s -wave [9],

$$\Phi_0^C(kr) = (kr)^{-1} \exp(i\sigma_0) F_0(\gamma; kr), \quad (10)$$

which is compared with the asymptotic Coulomb + strong wave function,

$$u_0(r; k) \stackrel{r \rightarrow \infty}{\equiv} \frac{e^{i\Delta_0}}{k} \left[F_0(\gamma; kr) \cos\hat{\delta}_0 - G_0(\gamma; kr) \sin\hat{\delta}_0 \right], \quad (11)$$

where $\gamma \equiv \mu_{K-d}\alpha/k$ is the Sommerfeld factor, F_0 and G_0 the s -wave regular and irregular Coulomb functions, and $\Delta_0 = \sigma_0 + \hat{\delta}_0$ the total phase shift. The latter includes two terms: $\sigma_0 = \arg(\Gamma(1+i\gamma))$ is the pure Coulomb phase shift (with Γ the Euler gamma function) and $\hat{\delta}_0$ the phase shift emerging from the strong interaction (similar, but not the same as δ_0). By performing a matching as in the Coulomb-free case, the expression for $\hat{\delta}_0$ can be computed as

$$\cot\hat{\delta}_0(k) = \frac{kRG_0'(\gamma; kR) - \beta_0(k)G_0(\gamma; kR)}{kRF_0'(\gamma; kR) - \beta_0(k)F_0(\gamma; kR)}. \quad (12)$$

D. Femtосcopy correlation function

The femtосcopy approach to measuring the strong interaction provides a spatio-temporal description of collisions at the femtometre scale [1] using as its basic observable the correlation function,

$$C_{\text{exp}}(k) = \xi(k) \frac{N_{\text{same}}(k)}{N_{\text{mixed}}(k)}, \quad (13)$$

or, in other words, the ratio (corrected for experimental effects by ξ) between the number of pairs recorded in the same event and pairs obtained by combining different collisions (mixed events), for a given reduced relative momentum, $k = |\frac{m_2\mathbf{k}_1 - m_1\mathbf{k}_2}{m_1+m_2}|$. It has been proven [10] that its theoretical equivalent,

$$C(k) = \int S(r) |\Psi(\mathbf{r}, k)|^2 d^3r, \quad (14)$$

measures the overlap between the source $S(r)$, which gives the relative position distribution of K^-d pairs for a given k , and the two-particle probability density $|\Psi(\mathbf{r}, k)|^2$ [1], [10]. Thus, it gives information either on the nature of the interaction between the particles and on the particle source. In this case, the latter is fixed as a spherical Gaussian distribution [3],

$$S(r) = \frac{1}{(2\pi R_{K-d}^2)^{3/2}} \exp\left(-\frac{r^2}{2R_{K-d}^2}\right), \quad (15)$$

where r is the relative distance between the pair and R_{K-d} is the size radius.

To observe how this technique helps to probe such short distances, it is useful to rewrite the wave function in the case of a strong spherically symmetric interaction at low energy as $\Psi(\mathbf{r}, k) = e^{i\mathbf{k}\cdot\mathbf{r}} - j_0(kr) + u_0^S(r; k)/r$, so that

$$C(k) = 1 + 4\pi \int S(r) \left(|u_0^S(r; k)|^2 - r^2 j_0^2(kr) \right) dr. \quad (16)$$

It is clear that $C(k)$ is sensitive to the difference between the interacting and free particle radial functions only where the source dominates, and so the signal will be significant in the region ranging from $R_{K-d} \sim 1 - 10$ fm (depending on the nuclei collision type and centrality), precisely where the strong interaction is at work. Its value will be related to the attractive ($C(k) > 1$), repulsive ($C(k) < 1$), or binding nature of the interaction, as shown in Ref. [2], since it depends on whether the correlated wave function is pushed in or out with respect to the free one. Femtосcopy is useful to understand low-energy phenomena in particular, since for high k (shorter de Broglie wavelengths), the intensity of the wave is lower and so the signal dies out and tends to 1, thus indicating no correlation.

Likewise, in interactions including the Coulomb force [9], the expansion of $\Psi(\mathbf{r}, k) = \Phi_{\text{tot}}^C(\mathbf{r}, \mathbf{k}) - \Phi_0^C(kr) + u_0(r; k)/r$ leads to

$$C(k) = \int S(r) |\Phi_{\text{tot}}^C(\mathbf{r}, \mathbf{k})|^2 d^3r + 4\pi \int S(r) \left[|u_0(r; k)|^2 - r^2 |\Phi_0^C(kr)|^2 \right] dr, \quad (17)$$

where the total Coulomb wave function is given by:

$$\Phi_{\text{tot}}^C(r, k, z) = e^{-\frac{\pi\gamma}{2}} \Gamma(1 + i\gamma) e^{ikz} {}_1F_1[-i\gamma; 1; ik(r-z)], \quad (18)$$

with $z = r \cos\theta$, θ the relative angle between \mathbf{r} and \mathbf{k} and ${}_1F_1$ the confluent hypergeometric function.

III. RESULTS

A. K^-d potential

The folding of the V_{K-p} and V_{K-n} local potentials over ρ_d , computed through a Gauss-Legendre quadrature method, produces the structure for the K^-d strong interaction at the threshold energy, $\sqrt{s} = m_K + m_d$, shown in Fig. 1.

The well's depth (~ 130 MeV for the real part) and range is a consequence of the potential folding (cf. Appendix B), which smoothens the effects of both the K^-p and K^-n strong interactions. Contributions to other coupled channels below threshold (such as the $\pi\Sigma$) are the reason behind the imaginary part of the potential.

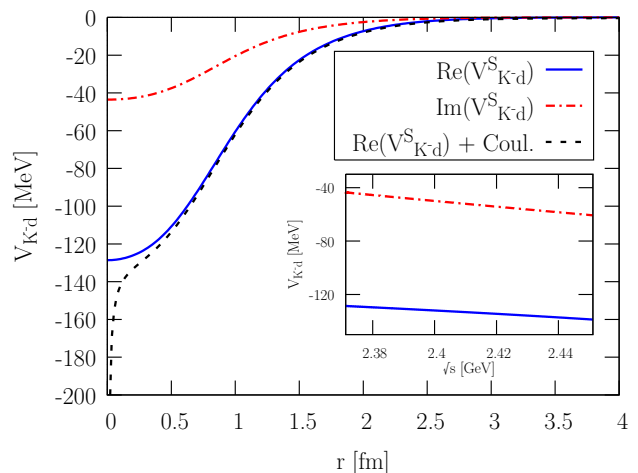


FIG. 1: Real (solid) and imaginary (dot-dashed) parts of the strong potential V_{K-d}^S at threshold $\sqrt{s} = 2371.28$ MeV. The dashed line represents the combined Coulomb and strong potentials. The inset shows the $V_{K-d}^S(\sqrt{s})$ dependence at $r = 0$.

B. Kaon-deuteron wave functions

The K^-d potential is now used to compute the wave functions by solving the SE. With the help of the aforementioned Numerov algorithm with step size $\Delta r = 0.0875$ fm, and of the routines to compute the Coulomb special functions in [11], the functions in Fig. 2 are obtained for several momenta. To better interpret them, they are divided by $\exp(i\Delta_0)$, so only $\hat{\delta}_0$ is in play with respect to F_0/k .

It can be observed, especially in the upper panel in which k is small, how $\text{Re}[u_0(r)]$ exhibits a fast turning point close to $r = 0$ fm: this is evidence of a bound state, which corresponds to the presence of the $\Lambda(1405)$ resonance right below the $\bar{K}N$ threshold, whose signal permeates into the K^-d interaction. This peak brings an asymptotic phase shift of about π close to $k = 0$, thus confirming Levinson's theorem [10] when a bound state is present. This phase shift decreases when k increases, as seen in the lower panel for a higher value of k , and tends to 0 at infinite momentum.

C. Femtосcopy correlation functions

The computed wave function is now used to calculate the pair correlation function and compare with available ALICE data for Pb+Pb collisions at $\sqrt{s_{NN}} = 5.02$ TeV [3]. Firstly, the total, strong and Coulomb correlation functions for different values of R_{K-d} are shown in Fig. 3 to analyse their behaviour.

At low k , the Coulomb attractive interaction, with $C(k) > 1$, dominates, as the integral of $|\Phi_{\text{tot}}^C|^2$ diverges at $k \rightarrow 0$. As k increases, the strong interaction dominates, giving rise to pockets with $C(k) < 1$ which mimic the

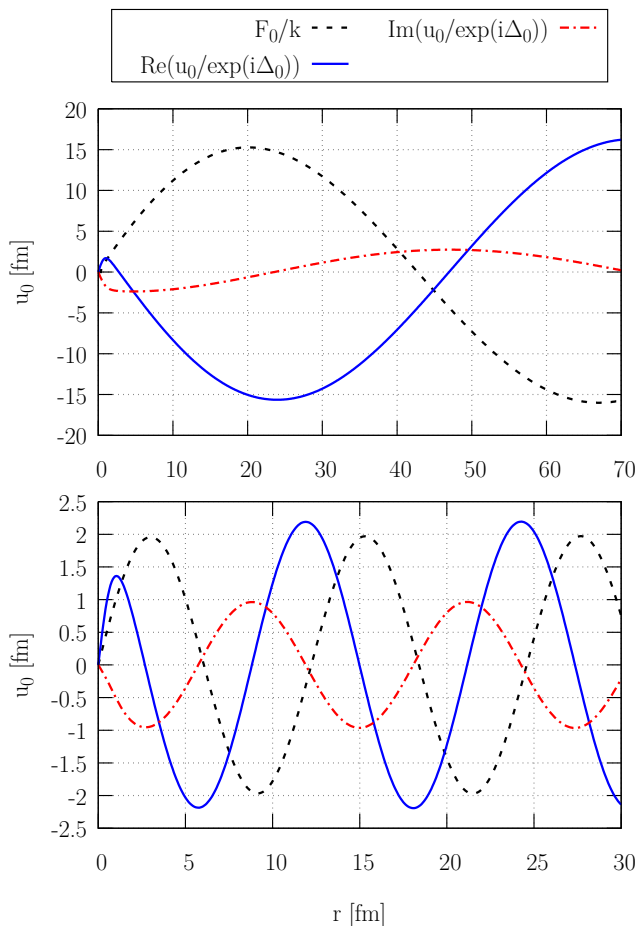


FIG. 2: Real (solid) and imaginary (dot-dashed) parts of the wave function $u_0(r)$, for $k = 12$ MeV (upper panel) and for $k = 100$ MeV (lower panel). The dashed line represents F_0/k .

effect of a repulsive interaction, but in fact are evidence of the existence of a bound state related to the presence of the $\Lambda(1405)$ in the $\bar{K}N$ interaction. As mentioned before, at high k , $C(k)$ becomes structureless.

The evolution of the correlation function with different R_{K-d} confirms the influence of this bound state, which is reflected in the enhancement of the wave function at short distances. Small values of the source (upper panel) are more sensitive to it and so $C(k) > 1$, even if for higher k , the subsequent decrease in $|u_0(r)|^2$ brings $C(k)$ below 1; it also tends to 1 more slowly as it takes longer to detect the following increase in the wave function oscillation.

Larger R_{K-d} (middle and lower panels) imply that the correlation function barely detects this confined enhancement, only the mentioned decrease in $|u_0(r)|^2$ that follows, so the pocket in $C(k)$ moves to lower momenta. For even larger values of R_{K-d} this shape will be retained, but with an increasingly lower signal, as the source will give more importance to the asymptotic region, up to the point where total correlation function will coincide with the long-range Coulomb one.

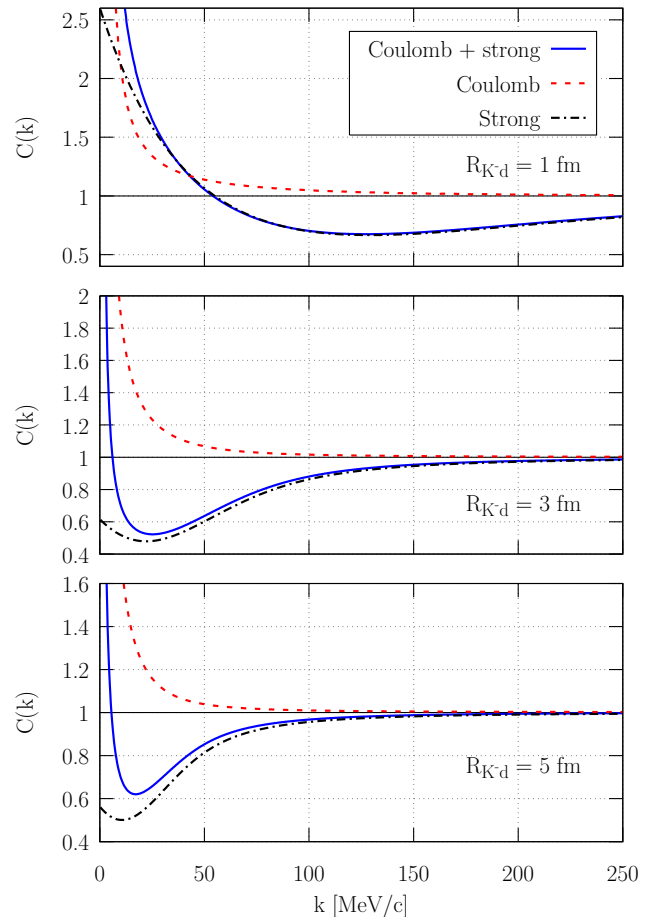


FIG. 3: Correlation functions of the total (solid line), Coulomb-only (dashed) and strong-only (dot-dashed) K^-d interactions for different values of R_{K-d} .

Finally, Fig. 4 probes this theoretical prediction with the experimental data. The numerical results use three different R_{K-d} which, following the fits in Ref. [3], are referenced to three different centrality classes that quantify the overlap between the colliding nuclei; low centrality (a full overlap) creates a larger source, and vice-versa. The agreement is impressive, considering V_{K-d} is obtained directly from the elementary $\bar{K}N$ interaction folded with the deuteron probability density. The regions of disagreement, such as the minima of the pockets, might be improved by a full consideration of the three-body K^-np problem, which is beyond the scope of this work. Furthermore, the R_{K-d} values given in [3] have in fact been extracted through a global fit of a source function and a low-energy interaction which does not necessarily coincide with our more sophisticated calculation. This means that there is still freedom to slightly modify these radii by a new fit that incorporates our realistic V_{K-d} interaction model. Finally, the use of higher partial waves could also help to fill the missing gap.

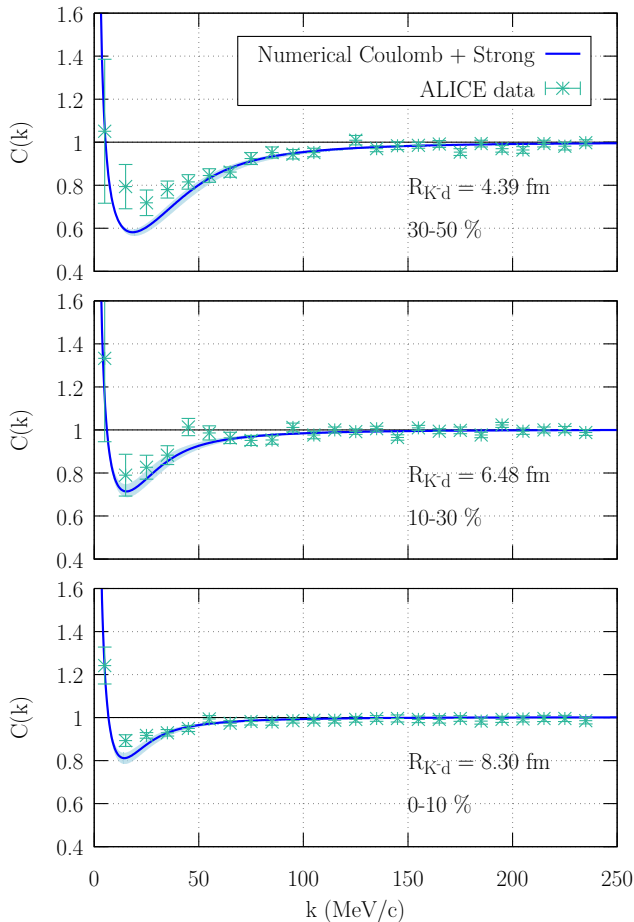


FIG. 4: Theoretical and experimental correlation functions [3] for $R_{K^-d} = 4.39^{+0.20}_{-0.29}$ fm (top), $6.48^{+0.58}_{-0.44}$ fm (middle), $8.30^{+0.58}_{-0.55}$ fm (bottom). Theoretical error bands come from the uncertainty of the source radii. The percentage ranges correspond to collision centrality.

IV. CONCLUSIONS

In this work, a novel approach has been implemented to describe the K^-d interaction through a potential folding of the kaon-proton and kaon-neutron single-channel equivalent potentials. A Fortran code has been developed to numerically solve the Schrödinger equation and compute its wave and correlation functions. There is excellent agreement between the prediction of the latter and ALICE experimental data for Pb-Pb collisions at three different collision centralities. Finally, a prediction of the K^-d correlation function in p-p collisions, where $R_{K^-d} \sim 1$ fm, is made available in Fig. 3 to compare with future experimental data.

A future path for improving the theoretical model could be to use a 3-body scheme, to include next-to-leading order terms in the Lagrangian or to go beyond the $l = 0$ approximation to check the convergence of higher partial waves. Additionally, the obtained interaction can be used for a global fit of the source radius using ALICE experimental data. Finally, computing the K^+d case in an analogous way could also be the focus of subsequent research; another interesting system in which there are recent experimental data is $\pi^\pm d$ [13]. Once this is done, the codes will be available at https://github.com/steve-cabre97/K_d_femtoscopic.git.

Acknowledgments

I would like to profoundly thank my two advisors, Àngels and Juan, for their constant help throughout this work and for the opportunity to discover, despite the constraints of time and my own lack of experience, a few of the fascinating aspects of current research in particle physics. I want to also mention Marc Piquer for his Numerov routine that I have adapted in my code. Finally, I must thank my family and friends for their support, and especially Jana for her encouragement and patience.

-
- [1] L. Fabbietti, V. Mantovani Sarti and O. Vázquez Doce, *Ann. Rev. Nucl. Part. Sci.* **77**, 1–28 (2021). <https://doi.org/10.1146/annurev-nucl-102419-034438>
 - [2] Z. Liu, J. Lu and L. Geng, *Phys. Rev. D* **107**, 074019 (2023), <https://doi.org/10.1103/PhysRevD.107.074019>
 - [3] W. Rzesza, "Non-identical particle femtoscopy of pairs containing deuteron and interaction studies of nucleons with strange matter", Ph.D. thesis, 2025. <https://repository.cern/records/w7g33-kpv15>
 - [4] E. Oset, A. Ramos, *Nuclear Physics A* **635**, 99-120 (1998). <https://doi.org/10.1016/S0375-9474>
 - [5] K. Miyahara, T. Hyodo, *Physical Review C* **93**, 015201 (2016). <https://doi.org/10.1103/PhysRevC.93.015201>
 - [6] K. Miyahara, T. Hyodo, W. Weise, *Phys. Rev. C* **98**, 025201 (2018). <https://doi.org/10.1103/PhysRevC.98.025201>
 - [7] G.R. Satchler, *Direct Nuclear Reactions* (Oxford University Press, Oxford 1983)
 - [8] M. Macêdo-Lima and L. Madeira, *Rev. Bras. Ens. Fis.* **45**, e20230079 (2023). <https://doi.org/10.1590/1806-9126-RBEF-2023-0079>
 - [9] C. J. Joachain, *Quantum Collision Theory*, (North-Holland Publishing Company, Amsterdam, 1975)
 - [10] M. Lisa, S. Pratt, R. Soltz, U. Wiedemann, *Annu. Rev. Nucl. Part. Sci.* **55**, 357-402 (2005), <https://doi.org/10.48550/arXiv.nucl-ex/0505014>
 - [11] F. Salvat, J. M. Fernandez-Varea, *Computer Physics Communications* **240**, 165-177 (2019)
 - [12] M. Mahlein, *et al.*, *Eur. Phys. J. C* **83**, 804 (2023). <https://doi.org/10.1140/epjc/s10052-023-11972-3>
 - [13] S. Acharya *et al.* [ALICE], <https://arxiv.org/abs/2504.02333>

Estudi de la femtoscopia del kaó-deuteró

Author: Esteve Cabré Coll-Vinent

Facultat de Física, Universitat de Barcelona, Diagonal 645, 08028 Barcelona, Spain.

Advisors: Juan Torres Rincón and Àngels Ramos

Resum: La interacció kaó-deuteró s'ha estudiat mitjançant diferents models. El que es desenvolupa en aquest treball construeix la interacció K^-d mitjançant el *fitting* de potencials locals K^-n i K^-p derivats d'un Lagrangian efectiu quiral. Aquest enfocament es posa a prova utilitzant la tècnica de la femtoscopia i les dades de la funció de correlació K^-d proporcionades per la col·laboració ALICE del LHC. Els resultats mostren una coincidència excel·lent amb les dades experimentals i proporcionen proves d'un estat quasi-lligat heretat de la ressonància $\Lambda(1405)$, a banda d'obrir la porta a millores del model per tal de restringir els valors físics de la font femtoscòpica.

Paraules clau: Teoria de col·lisions; femtoscopia; Equació de Schrödinger

ODS: Educació de qualitat; Indústria, innovació, infraestructures; Aliança pels objectius

Objectius de Desenvolupament Sostenible (ODS o SDGs)

1. Fi de les desigualtats		10. Reducció de les desigualtats	
2. Fam zero		11. Ciutats i comunitats sostenibles	
3. Salut i benestar		12. Consum i producció responsables	
4. Educació de qualitat	X	13. Acció climàtica	
5. Igualtat de gènere		14. Vida submarina	
6. Aigua neta i sanejament		15. Vida terrestre	
7. Energia neta i sostenible		16. Pau, justícia i institucions sòlides	
8. Treball digne i creixement econòmic		17. Aliança pels objectius	X
9. Indústria, innovació, infraestructures	X		

El contingut d'aquest TFG, part d'un grau universitari de Física, es relaciona amb l'ODS 4, i en particular amb la fita 4.4, ja que proveeix de competències a nivell universitari. També es pot relacionar amb l'ODS 9, fita 9.5, ja que contribueix a augmentar la investigació científica, i amb l'ODS 17, fita 17.6, ja que promou l'intercanvi de coneixements científics.

Appendix A: SINGLE-CHANNEL EQUIVALENT POTENTIAL

In the original $\bar{K}N$ scattering problem, the T -matrix approach is a coupled-channel problem with 4 channels ($\bar{K}N, \pi\Sigma, \eta\Lambda, K\Xi$) in the $I = 0$ case and 5 channels ($\bar{K}N, \pi\Sigma, \pi\Lambda, \eta\Sigma$ and $K\Xi$) in the $I = 1$ case. Therefore, the T -matrix equation that sums up all channels reduces to a matrix equation. The equivalent Schrödinger problem would also be a system of coupled differential equations.

Since a single Schrödinger equation is to be implemented, a single-channel equivalent potential for the $\bar{K}N$ scattering needs to be found, such that the T_{11} matrix element is exactly equal to the one obtained in the full coupled-channel problem.

To start with, the leading order χ EFT Lagrangian provides the lowest order scattering amplitude V_{ij} , while G_l is the meson-baryon propagator, which is diagonal as it describes propagation between vertices. First, the simple 2×2 case is sketched, and finally the general formula given in Refs. [5, 6] is provided. With 2 scattering channels, the V and G matrices read,

$$V = \begin{pmatrix} V_{11} & V_{12} \\ V_{21} & V_{22} \end{pmatrix}, \quad G = \begin{pmatrix} G_1 & 0 \\ 0 & G_2 \end{pmatrix}. \quad (\text{A1})$$

The T -matrix equation $T = V + VGT$ is solved via matrix inversion,

$$T = (1 - VG)^{-1}V. \quad (\text{A2})$$

Focusing on the 11 channel, the explicit solution is straightforward,

$$\begin{aligned} T_{11} &= \frac{V_{11} - V_{11}V_{22}G_2 + V_{12}V_{21}G_2}{1 - V_{22}G_2 - V_{11}G_1 + V_{11}V_{22}G_1G_2 - V_{12}V_{21}G_1G_2} \\ &= \frac{1}{\frac{1 - V_{22}G_2}{V_{11} - V_{11}V_{22}G_2 + V_{12}V_{21}G_2} - G_1}. \end{aligned} \quad (\text{A3})$$

Since the aim is a single channel equation, a V_{11}^{eff} , yet to be determined, is now defined such that

$$T_{11} = \frac{1}{(V_{11}^{\text{eff}})^{-1} - G_1}. \quad (\text{A4})$$

Then, matching Eqs. (A3) and (A4), the following expression is obtained:

$$V_{11}^{\text{eff}} = V_{11} + V_{12}G_2V_{21} + V_{12}G_2\tilde{T}_{22}G_2V_{21}, \quad (\text{A5})$$

where \tilde{T}_{22} is defined as the reduced T -matrix of the 22 problem,

$$\tilde{T}_{22} \equiv \frac{1}{V_{22}^{-1} - G_2}. \quad (\text{A6})$$

In this way, the single-channel potential V_{11}^{eff} gives rise to the same T_{11} matrix element obtained by the solution

to the 2×2 problem. In the multichannel problem, the expression can be generalized to [3, 4],

$$V_{11}^{\text{eff}} = V_{11} + \sum_{m=2}^N V_{1m}G_mV_{m1} + \sum_{m,l=2}^N V_{1m}G_m\tilde{T}_{ml}G_lV_{l1}. \quad (\text{A7})$$

Appendix B: POTENTIAL FOLDING FOR V_{K-d}

The starting point are the potentials V_{K-p} and V_{K-n} in the charge basis obtained by multiplying the effective potentials provided by Àngels Ramos's code, already multiplied by $N(\sqrt{s})$ by $g(r)$,

$$V_{K-n,p}(r, \sqrt{s}) = g(r)N(\sqrt{s})V_{11}^{\text{eff}}(\sqrt{s}). \quad (\text{B1})$$

The plots in Fig. 5 are obtained, which show deep and narrow potential wells; this is due to the addition of the Gaussian radial dependence, which is a regularization of the Dirac delta potential, coming from a local, zero-range form of the obtained T -matrix.

Then, following the procedure outlined in Ref. [7], the two potentials are convoluted with the deuteron probability density, $\rho_d(r')$, and added in the following way,

$$\begin{aligned} V_{K-d}^S(r, \sqrt{s}) &= \int d^3r' \rho_d(r') \left[V_{K-p}(|\mathbf{r} - \frac{1}{2}\mathbf{r}'|, \sqrt{s}) \right. \\ &\quad \left. + V_{K-n}(|\mathbf{r} + \frac{1}{2}\mathbf{r}'|, \sqrt{s}) \right], \end{aligned} \quad (\text{B2})$$

where \mathbf{r}' is the relative distance between the proton and the neutron, and \mathbf{r} is the distance between the kaon and the center of mass of the proton and the neutron, as shown in Fig. 6. In this way, $\rho_d(r')$ limits the strength of the potential as it suppresses the region where V_{K-i} is strongest due to the $b = 0.52$ fm parameter in $g(r)$. The folding thus provides a measure of exclusion radius to the theoretical prediction, while increasing its range due to the sum of both potentials.

The density $\rho_d(r)$ encodes the deuteron wave function squared, both in s - and d - wave components, and is provided by a routine implementing the parametrization given in Ref. [12], a function fitted to the solution of the SE for the Argonne v_{18} potential, and its normalization is,

$$\int_0^\infty dr r^2 \rho_d(r) = 1. \quad (\text{B3})$$

Rewriting the first argument of V_{K-p} and V_{K-n} gives

$$\begin{aligned} V_{K-p}(|\mathbf{r} - \frac{1}{2}\mathbf{r}'|, \sqrt{s}) &= V_{K-p} \left(\sqrt{r^2 + \frac{1}{4}r'^2 - rr'x}, \sqrt{s} \right), \\ V_{K-n}(|\mathbf{r} + \frac{1}{2}\mathbf{r}'|, \sqrt{s}) &= V_{K-n} \left(\sqrt{r^2 + \frac{1}{4}r'^2 + rr'x}, \sqrt{s} \right), \end{aligned} \quad (\text{B4})$$

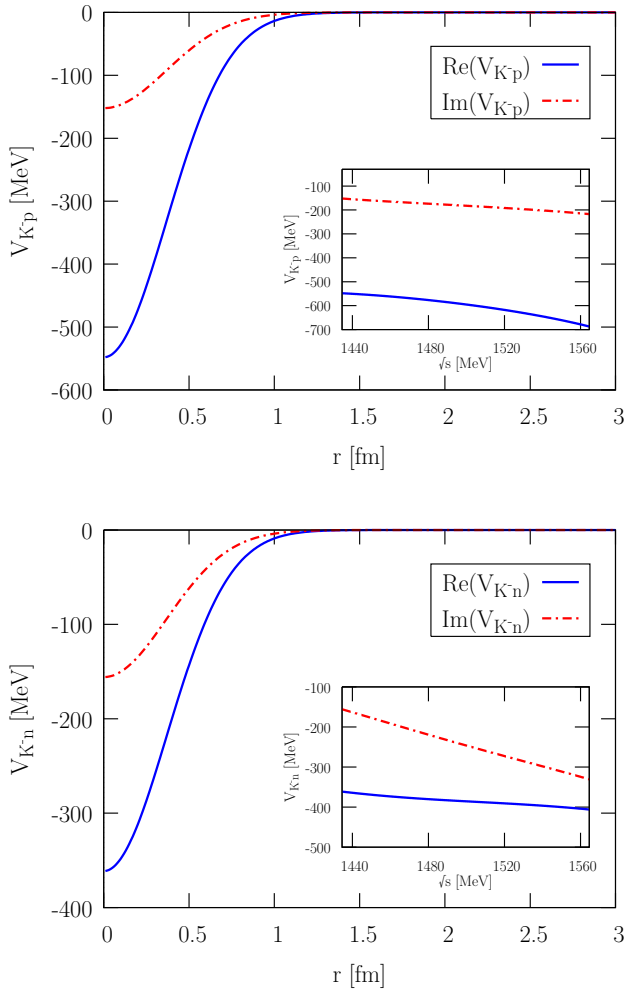


FIG. 5: The main plot shows the radial dependence of potentials V_{K-p} (upper panel) and V_{K-n} (lower panel) at threshold $\sqrt{s} = 1434.591$ MeV, while the inset plot show the energy dependence at $r = 0$ fm.

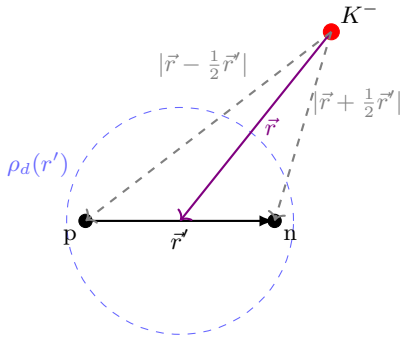


FIG. 6: Figure of a K^- interacting with a deuteron (pn pair), with the deuteron probability density $\rho_d(r')$.

where $x = \cos \theta$ and θ is the angle between \mathbf{r} and \mathbf{r}' . For the integral in Eq. (B2), the energy-dependent part can be factorized out, and the radial-dependent part, being

spherically symmetric, is the same for both particles. The Gauss-Legendre quadrature procedure is thus applied to integrate for x and r' only once, and the result multiplied by the sum of the energy dependent parts for the proton and the neutron,

$$V_{K-d}^S(r) \approx \sum_i^{n_r} w_i \rho(x_i) x_i^2 \sum_j^{n_x} h_j g \left(\sqrt{r^2 + \frac{1}{4} x_i^2 - r x_i y_j} \right)$$

$$V_{K-d}^S(r, \sqrt{s}) = V_{K-d}^S(r) N(\sqrt{s}) \left[V_{K-p}^{\text{eff}}(\sqrt{s}) + V_{K-n}^{\text{eff}}(\sqrt{s}) \right], \quad (\text{B5})$$

where x_i and y_j are the nodes and w_i and h_j the Gaussian weights for the integrals in r' and x , respectively.